AD-A126 269 LASER INTERACTION WITH METALLIC SURFACES(U) POLYTECHNIC 1/
INST OF NEW YORK FARMINGDALE MICROWAVE RESEARCH INST
W T WALTER DEC 82 POLY-MRI-1425-82 N00014-78-C-0678

UNCLASSIFIED F/G 20/5 NL

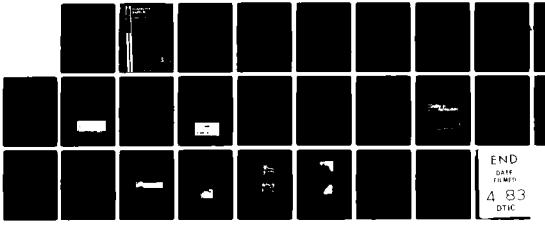

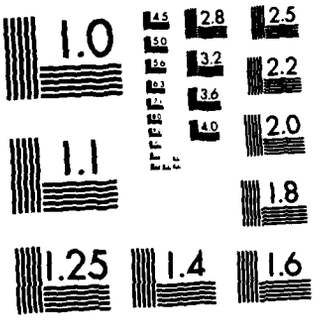

Polytechnic Institute of New York
MICROWAVE RESEARCH INSTITUTE

(12)

POLY-MRI-1425-82
December 1982

LASER INTERACTION WITH METALLIC SURFACES

by

William T. Walter

Final Technical Report

Prepared for
OFFICE OF NAVAL RESEARCH
Contract No. N00014-78-C-0678

Unclassified

SECURITY CLASSIFICATION OF THIS PAGE (When Data Entered)

REPORT DOCUMENTATION PAGE		READ INSTRUCTIONS BEFORE COMPLETING FORM
1. REPORT NUMBER	2. GOVT ACCESSION NO. AD-A126769	3. RECIPIENT'S CATALOG NUMBER
4. TITLE (and Subtitle) Laser Interaction with Metallic Surfaces		5. TYPE OF REPORT & PERIOD COVERED Final Technical Report Sept. 1, 1978-Aug. 31, 1981
		6. PERFORMING ORG. REPORT NUMBER POLY-MRI-1425-82
7. AUTHOR(s) William T. Walter		8. CONTRACT OR GRANT NUMBER(s) N00014-78-C-0678
9. PERFORMING ORGANIZATION NAME AND ADDRESS Polytechnic Institute of New York Microwave Research Institute Route 110, Farmingdale, New York 11735		10. PROGRAM ELEMENT, PROJECT, TASK AREA & WORK UNIT NUMBERS
11. CONTROLLING OFFICE NAME AND ADDRESS Office of Naval Research 800 North Quincy Street, Code 431 Arlington, Virginia 22217		12. REPORT DATE December 1982
		13. NUMBER OF PAGES
14. MONITORING AGENCY NAME & ADDRESS(if different from Controlling Office)		15. SECURITY CLASS. (of this report) Unclassified
		15a. DECLASSIFICATION/DOWNGRADING SCHEDULE

16. DISTRIBUTION STATEMENT (of this Report)

Approved for public release; distribution unlimited.

17. DISTRIBUTION STATEMENT (of the abstract entered in Block 20, if different from Report)

18. SUPPLEMENTARY NOTES

19. KEY WORDS (Continue on reverse side if necessary and identify by block number)

Laser-Material Interraction, Optical Properties, Reflectance, Metals, Copper, Laser, Drude Model, Vapor-Deposited Copper, Polycrystalline Copper, Diamond-Turned Copper, Copper Spectral-Emission Lines, Microstructural Effects, Shock Deformation, Crater Formation, Void Formation, Ripple Patterns, Twinning.

20. ABSTRACT (Continue on reverse side if necessary and identify by block number)

Direct real-time measurements of a target material's optical properties with subnanosecond resolution may provide crucial, process-revealing signatures in following the interaction of an intense laser beam with a metal as the surface progressively undergoes heating, plastic deformation, slip, vaporization, ejection of liquid metal, plasma formation, etc. Three classes of physical processes have been proposed to account for a substantial decrease in reflectance observed during the interaction of an intense laser pulse with

DD FORM 1 JAN 73 1473 EDITION OF 1 NOV 65 IS OBSOLETE

Unclassified

SECURITY CLASSIFICATION OF THIS PAGE (When Data Entered)

a metal surface: (1) deformation of the surface, (2) plasma formation, and (3) a nonlinear process causing enhanced absorption within the metal. Thus far we may conclude that specular reflectance is a sensitive indicator of surface deformation. Total reflectance measurements, on the other hand, indicate that until the surface temperature of a metal target reaches the vicinity of the boiling point, the total reflectance does not differ significantly from that given by a Drude-type free-electron model. The reflectivity decrease of a Drude model for a metal heated from room temperature to a liquid at the boiling point is not large enough to account for the substantial reflectance decrease observed experimentally. The effect of different target material structures, such as single-crystal, vapor-deposited, annealed with different grain sizes, bulk polycrystalline, cold-rolled with high dislocation density, diamond-tuned, etc., were examined using copper as the basic target material. Differences were detected between the dynamic reflectance behavior of each. Vapor deposited copper targets showed the minimum decrease in reflectance during the laser pulse, closely followed by diamond-turned copper surfaces. Polycrystalline, cold-rolled copper, targets exhibited the greatest decrease in reflectance. In addition to reflectance measurements, spectral measurements have begun on the plasma which forms in front of a copper surface at incident laser power densities above $3 \times 10^8 W/cm^2$. Spectral emission lines have been observed from neutral copper atoms, ions and dimers (Cu_2) in the plasma when the surface temperature of copper exceed the boiling point.

Microstructural analysis of the targets also revealed differences between the laser-material interaction for different copper target preparations. For vapor-deposited copper surfaces, small drops of liquid were ejected and a ring of voids formed outside the crater. Vacuum-annealed vapor-deposited samples showed larger drops of liquid metal ejected and no ring of voids. Instead, a ripple pattern formed outside the edge of the crater generated by the transverse component of the shock wave. In tin targets, the wavelength of the ripple pattern decreased gradually from the crater edge outward. Heavy twinning occurred near the crater edge in tin and zinc targets. In zinc targets, because of different crystallographic orientation of the grains, ripple patterns occurred in one grain, while an adjacent grain was twinned. Grain boundaries acted as barriers to the propagation of deformation processes. When target samples were chemically etched, preferential melting appeared to take place along the grain boundaries.

TABLE OF CONTENTS

REPRINTED FROM PROCEEDINGS OF THE INTERNATIONAL CONFERENCE ON LASERS '81, DECEMBER 14-18, 1981
PRINTED IN USA

OPTICAL PROPERTIES OF METAL SURFACES DURING LASER IRRADIATION

W. T. Walter, N. Solimene, K. Park, T. H. Kim and K. Mukherjee

Departments of Electrical Engineering/ Computer Science and
Physical Metallurgy and Microwave Research Institute
Polytechnic Institute of New York
Route 110
Farmingdale, N.Y. 11735

Abstract

Direct real-time measurements of a target material's optical properties with subnanosecond resolution may provide crucial, process-revealing signatures in following the interaction of an intense laser beam with a metal as the surface progressively undergoes heating, plastic deformation, slip, vaporization, ejection of liquid metal, plasma formation, etc. Three classes of physical processes have been proposed to account for a substantial decrease in reflectance observed during the interaction of an intense laser pulse with a metal surface: (1) deformation of the surface, (2) plasma formation, and (3) a nonlinear process causing enhanced absorption within the metal. Thus far we may conclude that specular reflectance is a sensitive indicator of surface deformation. Total reflectance measurements, on the other hand, indicate that until the surface temperature of a metal target reaches the vicinity of the boiling point, the total reflectance does not differ significantly from that given by a Drude-type free-electron model. The reflectivity decrease of a Drude model for a metal heated from room temperature to a liquid at the boiling point is not large enough to account for the substantial reflectance decrease observed experimentally. In addition to reflectance measurements, spectral measurements have begun on the plasma which forms in front of a copper surface at incident laser power densities above 3×10^8 W/cm^2. Spectral emission lines have been observed from neutral copper atoms, ions and dimers (Cu_2) in the plasma when the surface temperature of copper exceeds the boiling point.

Introduction

Real-time monitoring of the material parameters during a laser-material interaction can improve our understanding of the physical processes involved and enable us to follow the transfer of energy from an incoming laser beam to the target material. Since bandwidths of optical detection systems exceed one gigahertz, optical measurements can be readily carried out on a subnanosecond time scale. The optical properties of a substance, therefore, merit special consideration because they are quantities that can be measured directly with subnanosecond resolution. Optical properties include the scalar quantities: absorptance, transmittance, and reflectance as well as the complex or vector quantities: dielectric constant, refractive index and conductivity. Although we would like to measure directly other properties such as surface and bulk temperatures on such a fast time scale, temperature is extremely difficult to measure directly even on a microsecond time scale. Therefore, in following the interaction of an intense laser beam with a target material, such as a metal, real-time measurements of the optical properties of the metal may differentiate and be process-revealing. Since for opaque targets the absorptance is one minus the reflectance, measurement of the time dependence of the metal surface reflectance will yield the laser power directly deposited into the metal. The absorbed power can then be used to calculate the metal's temperature history during and following laser irradiation. Our goal is to measure and then use the optical properties of metals to develop a better understanding of the laser interaction from heating through to plasma formation. At present, polarimetric or ellipsometery measurements have not yet been carried out during laser interaction experi-

ments. Hence in this paper, we will concentrate on the scalar optical properties of reflectance and absorptance as well as refractive index, plasma and electron-phonon collision frequencies which may be derived from these measurements. Our long range goal is to measure these quantities directly as well as to carry out spectroscopic measurements of populations and temperatures in the plasma produced at the metal surface.

Target Reflectance Behavior

Experimentally, the reflectance of a metal surface has been observed to undergo a sharp and substantial decrease during an intense laser pulse.[1-11] For incident laser power densities above threshold values which lie between 10^7 and 10^9 W/cm^2, the measured reflectance of a metal surface drops significantly before partially or totally recovering as indicated by the curves in Figure 1a. This type of reflectance change was first reported by Bonch-Bruevich et al.[1] during individual spikes ≈400-ns FWHM (Full Width at Half-Maximum intensity) within a millisecond 1.06-μ Nd glass laser pulse on targets of silver, copper, aluminum, dural and steel as indicated.

There are three distinct regions within a generalized reflectance curve as illustrated in Figure 1b: first, AB - an initial steep decrease to ≈one-half of the initial reflectance; second, BC or BC' - a plateau region during which the reflectance remains approximately constant; and third, C'D' - a complete reflectance recovery, or for higher intensity laser pulses CD, a further decrease to ≈one-tenth of the initial reflectance followed by a partial recovery.

Zavecz, Saifi and Notis[4] reported similar reflectance curves during Q-switched 1.06-μ Nd:YAG laser pulses ≈60-ns FWHM on single crystal copper and tantalum targets as shown in Figure 1c. The remarkably close agreement between Zavecz's 0.64 plateau reflectance value and the 0.66 value of Bonch-Bruevich for copper, the only metal common to both investigations, is evident in Figure 1. Plateau features have also been reported by Dymshits[8], using a 30-ns FWHM 1.06-μ Nd glass single laser pulse on thin alumuminum films, and Walters and Clauer[10], using gain-switched 50 to 70-ns 10.6-μ TEA CO_2 laser pulses on polished polycrystalline aluminum rods.

Bonch-Bruevich et al.[1] associated the initial steep decrease in the reflectance curve,

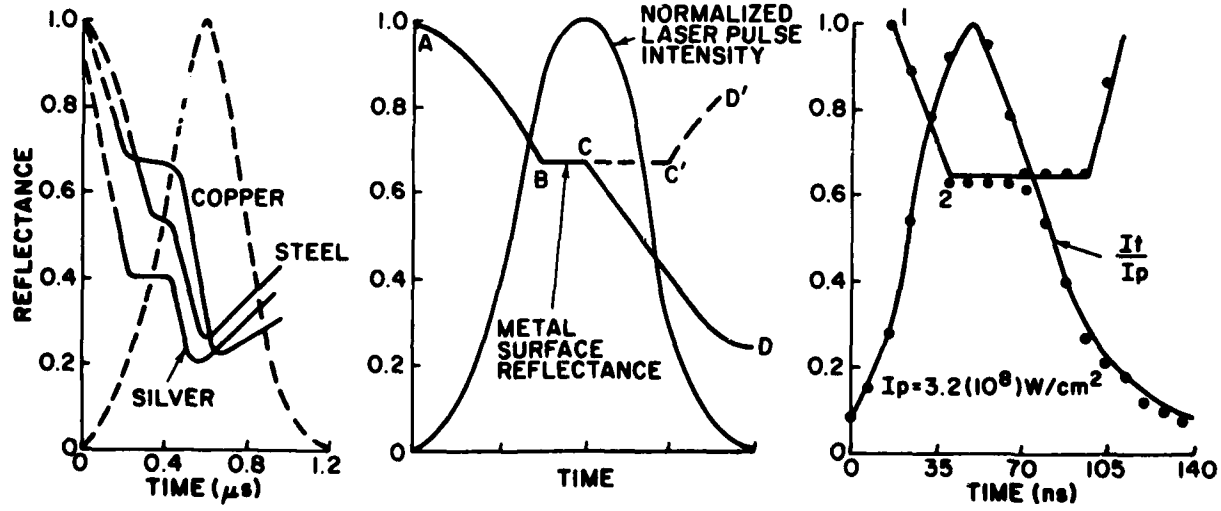

(a) REFLECTANCE MEASUREMENTS OF BONCH-BRUEVICH et al

(b) GENERAL REFLECTANCE CURVE

(c) REFLECTANCE MEASUREMENT OF ZAVECZ et al

Fig. 1 - Metal Reflectance Behavior during an intense laser pulse.

AB, with the heating of the metal surface to melting and with the drop in electrical conductivity which accompanies melting. The plateau BC or BC', they suggested, indicated that the temperature of the molten layer remained constant while the absorbed radiant energy propagated a melting wave into the solid. The further reflectance drop during region CD was attributed to a decrease in the amount of energy conducted to the liquefaction wavefront and, therefore, indicated a second region of increasing temperature.

Zavecz et al.[4] tested Bonch-Bruevich's conjecture that the metal was melting during region BC. A single-crystal copper target was irradiated with a laser intensity ($3.2 \times 10^8 W/cm^2$) which was sufficient to attain the plateau reflectance BC, as shown in Fig. 1c, but not high enough to cause the second reflectance decrease. Examination of the target by scanning electron beam microscopy revealed no evidence of melting. Melting occurred during the second decrease in reflectance, CD of Fig. 1b. A major difference between the two experiments was the use of an integrating sphere by Bonch-Bruevich and, therefore, a total reflectance measurement while Zavecz et al. measured only the specular reflectance. In ensuing experiments to Zavecz's, Koo and Slusher[5] proposed that the reflected beam could have been deflected into a wide cone of angles by a transient grating structure produced on the metal target surface. Ready[6] using a 10.6-μ CO_2 laser, and von Allmen[9] using a 1.06-μ Nd laser on metal targets, found substantial and permanent changes from specular to diffuse reflectance during the laser pulse. Ready used a probe laser to subtract plasma absorption and concluded that no recovery of reflectance occurred during or after the pulse. An ellipsoidal light collector was employed by von Allmen in front of a target in air. He found no significant change in the total reflectance until the metal surface temperature exceeded the boiling point. Prokhorov et al.[3] suggested the formation of a liquid dielectric layer causing an enhanced absorption. More recently, Dymshits[8] observed Fig. 1-type reflectance changes during a specular reflectance measurement with the metal target film in vacuum. He suggested that the reflection takes place from a plasma formation in front of the metal surface. Walters and Clauer[10] report a sharp decrease to ~0.35 in specular reflectance at the melting point of Al followed by nearly complete recovery. No luminosity was observed and no significant permanent loss of the high specular reflectance was detected.

An understanding of the metal surface reflectance behavior during an intense laser pulse is lacking at present. In addition to Bonch-Bruevich's suggestion that the initial steep decrease in reflectance is associated with the heating of the metal surface to melting, three classes of alternate explanations have been offered for the steep decrease in metal target reflectance during an intense laser pulse: 1) surface deformation, 2) plasma formation, or 3) nonlinear process. Before discussing these, we shall first examine the change in reflectance expected when a metal is heated to its melting point.

Free Electron Model

The Fresnel expression for the reflectivity, R, of radiant intensity at normal incidence on the surface of a homogeneous substance is[12, 13]

$$R = \frac{|\tilde{n}-1|^2}{|\tilde{n}+1|^2}$$

where $\tilde{n}$ is the complex refractive index. From the viewpoint of optics, the complex index of refraction may be expressed in terms of the optical constants n and k of the material

$$\tilde{n} = n - ik$$

where n is the index of refraction and k is the extinction coefficient.

In the Drude or free electron model, a metal is viewed as a gas of free electrons interacting with a background positive-ion lattice represented by phonons. The complex index of refraction then may be expressed in terms of the plasma frequency

$$\omega_p \equiv \sqrt{4\pi Ne^2/m^*},$$

the average electron-phonon collision frequency $\equiv \nu_c$ and the frequency of the incident light $\omega_{light} \equiv 2\pi c/\lambda$,

$$\tilde{n} = 1 - \frac{\omega_p^2}{\omega_{light}^2 + \nu_c^2}\left[1 + i\,\frac{\nu_c}{\omega_{light}}\right] = 1 - \frac{1}{\omega^2+\nu^2}\,(1+i\tfrac{\nu}{\omega})$$

where $\omega \equiv \omega_{light}/\omega_p$, and $\nu \equiv \nu_c/\omega_p$. Here N is the free eletron density, m^* is the effective mass of a free electron in the metallic lattice, e is the electronic charge and $i \equiv \sqrt{-1}$. For visible light incident on a good conductor

$$\omega_p \simeq 10^{16}\text{sec}^{-1} > \omega_{laser} \simeq 10^{15}\text{sec}^{-1} > \nu_c \simeq 10^{14}\text{sec}^{-1}.$$

Therefore, $\omega \simeq 10^{-1}$ and $\nu \simeq 10^{-2}$.

When the temperature is raised to the melting point, no significant change in the free electron density is expected for a metal whose bandgap is much greater than the thermal energy change. Therefore, no appreciable change is expected in the plasma frequency ω_p. The phonon density, however, may increase significantly and hence also may the electron-phonon collision frequency and ν. Figure 2 shows the dependence of the Fresnel reflectivity on the collision frequency for neodymium and ruby laser frequencies normally incident on a copper surface.

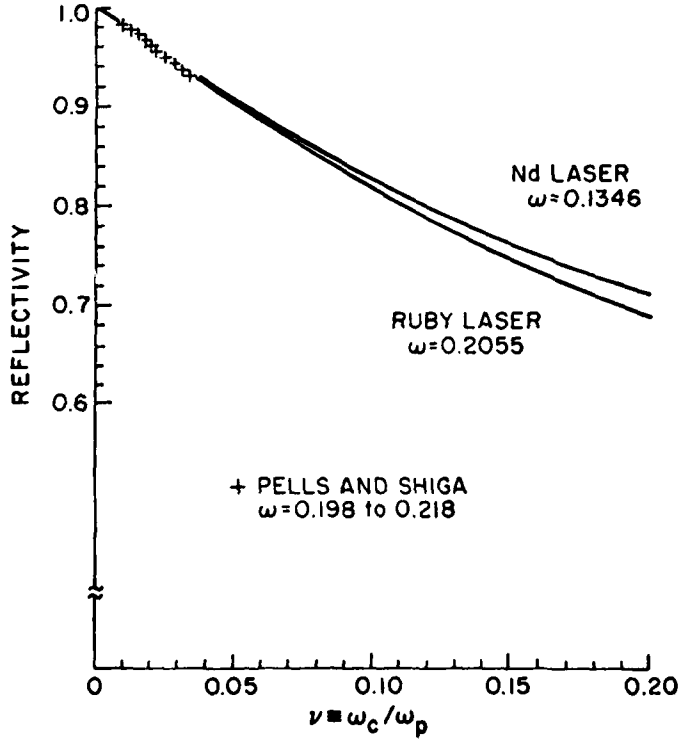

Fig. 2 - Reflectivity of Copper as a function of the electron-phonon collision frequency ν_c for two incident laser frequencies ω

There has been considerable variation in the room-temperature reflectance measurements of many metals. Since the absorption depth, $\lambda/2\pi k$, is only a few hundred angstroms at most for metals in the visible-near infrared spectral region, the measured reflectances of metals are very sensitive to the method of preparation of the surface as well as to the history of the surface from preparation to measurement. When the metallic surface is produced by polishing, mechanical stress can deform the surface by producing an amorphous layer which may be several hundred angstroms thick[14]. Even more detrimental is the embedding of polishing-compound particles which is more likely to take place in soft metals: copper, aluminum, etc. If an oxide layer is allowed to form, the reflectance measured will not be that of the pure metal. For metals which are good conductors and therefore also possess high reflectivities, processes which modify the metal-air or metal-vacuum interface generally reduce the reflectance. The highest reflectances of metals have been measured for evaporated coatings prepared in a high vacuum at a high rate of deposition of the metal and measured immediately after preparation while still in a high vacuum.[15] Reflectances of Ag, Cu and Al measured under these conditions at 1.06μ are .994, .985, and .944, respectively.

Figure 2 indicates that for a room-temperature copper reflectivity of 0.985 at 1.06μ, the ratio of the electron-phonon collision frequency to the plasma frequency $\nu = 0.00749$. According to the free electron model then, for the reflectivity of copper to decrease to 75%, for example, ν must increase so that $\nu > 0.15$. This implies that the electron-phonon collision frequency has increased more than 20 times.

Ujihara[13] has examined the temperature dependence of a Drude-type free-electron model for high conductivity metals. He asked whether the increase with temperature of the electron-phonon collision frequency can account for a reflectance decrease to the plateau value by the time that the metal reaches its melting point. Ujihara assumed a Debye model for the phonon spectrum and N-scattering processes on a spherical Fermi surface. Both the Debye temperature and the electron distribution were considered to be independent of temperature in the 300°K to melting point region. Ujihara's results for several metals at ruby and Nd wavelengths are shown in Figure 3. The reflectivity of solid copper at 1.06μ decreases from 0.95 at room temperature to 0.73 at the melting point, 1356°K. Since the conductivity of copper, like many other metals, decreases by a factor of 2 upon melting,[16] a reflectance of 0.58 would be expected for liquid copper at 1.06μ at the melting point. These reflectance values bracket the plateau reflectances of 0.66 and 0.64 observed by Bonch-Bruevich and Zavecz, and suggest that a Drude-type free-electron model may be able to explain the reflectance behavior observed. Indeed, as shown in Figure 4, Chan et al.[7] claim to have confirmed Ujihara's theoretical reflectivity curves using a ruby laser on copper and aluminum targets and calculating the surface temperature on the basis of a one-dimensional heat flow model.

Ujihara's analysis has been examined by Walter,[17] who pointed out that Ujihara, in his determination of the plasma frequency ω_p, used the 1913 effective mass measurements.[18] For copper, the old value is almost two times the more recent measurements. When the resulting low value for the plasma frequency was used with values of the optical constants, n and k, the room-temperature value Ujihara calculated for the electron-phonon collision frequency was 2.5 times too high and the room temperature reflectivity at 1.06μ was 95.2% instead of 98.5%. With these incorrect initial values, his analysis then predicted substantial changes in the collision frequency and in the reflectivity which are not confirmed by experiment, as indicated in Figure 5.

The solid curve in Figure 5 shows the temperature dependence of the reflectivity of copper calculated by Ujihara. The dotted curve extends Ujihara's analysis down to 77°K. The optical properties of copper have been measured polarimetrically in ultra-high vacuum ($\sim 10^{-9}$ Torr) by Pells and Shiga[19] over the temperature range 77 to 920°K. Reflectances computed from Pells and Shiga's experimental values of n and k are also indicated in Figure 5. The discrepancy between theory and experiment is substantial. However, when the improved data listed in Table I is used, then the theory of Ujihara is in much better

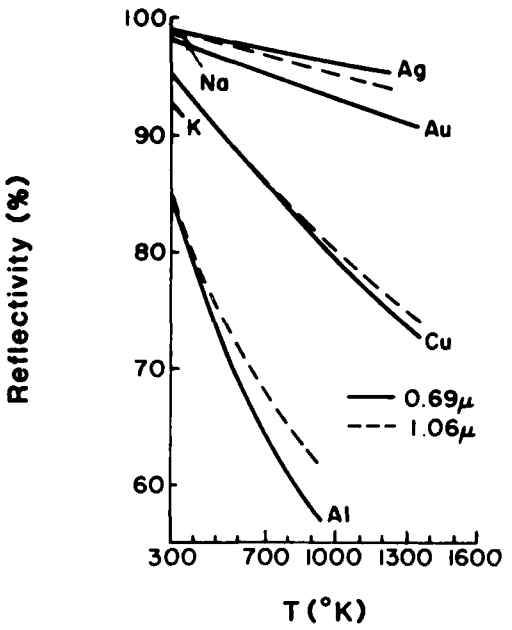

Fig. 3 - Ujihara's Calculated Reflectivities[13] for several metals at two laser frequencies.

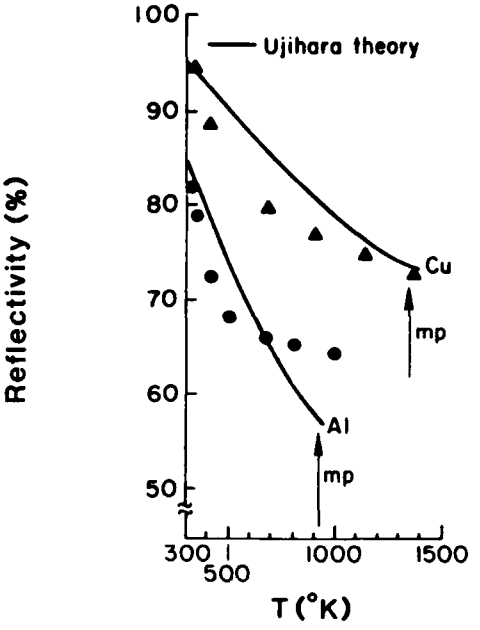

Fig. 4 - Chan's Measured Reflectances[17] of copper (triangles) and aluminum (dots) at 0.69μ.

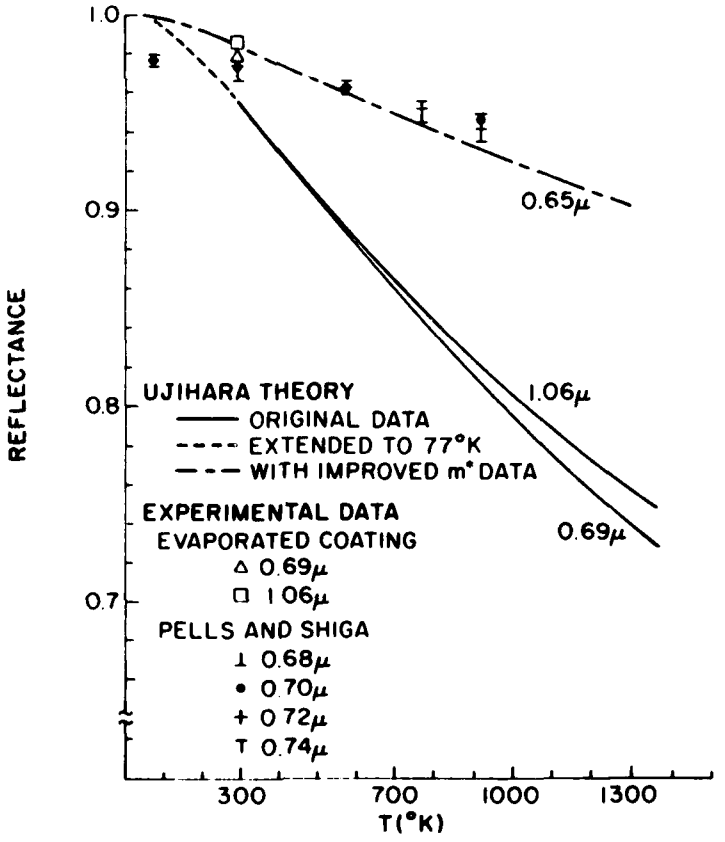

Fig. 5 - Temperature Dependence of the Reflectance of Copper.

agreement with Pell and Shiga's experimental results. The dominant change responsible for most of the improvement is Schulz's careful determination[20] of the effective electron mass in copper including a correction for the anomalous skin effect.

Table I. Input Data for Ujihara Theory

Parameter		Original Ujihara Analysis	Improved Data of Reference 17
Index of refraction	n	0.150[a]	0.1074[b]
Extinction coefficient	k	4.049[a]	3.9104[b]
Wavelength	λ	0.70 μ[a]	0.65 μ[b]
Effective mass	m^*/m	2.56[c]	1.45[d]

[a]Reference 21.
[b]Reference 22.
[c]Reference 18.
[d]Reference 20.

With these improvements in the input data used in the Ujihara theory, Walter concluded:

(1) the reflectance of liquid copper[23] is ~85%, not ~65%, and

(2) it is unlikely that the temperature dependence of a Drude-type free-electron model can explain the substantial reflectance changes reported high-conductivity metals such as copper.[17]

In Figures 6a and 6b, the temperature dependence of the optical constants n and k, and the free-electron model constants ω_p and ν_c, are displayed and compared with the polarimetric measurements of Pells and Shiga. As expected, it is evident that the plasma frequency does not change significantly with temperature. The plasma frequency can be determined from the optical constants n and k or from the free electron density and effective mass N and m^*. When the most precise n and k values[22] are used to determine ω_p values for Ag, Cu and Au, good agreement is obtained with ω_p values determined from N and m^*, using the effective mass values of Schulz. Also, the effective mass for electrons in Cu determined by Schulz from optical properties at 2 μ is nearly identical to the value from electronic specific heat determinations.[20] It is also evident in Fig. 6b that the electron-phonon collision frequency undergoes a much smaller increase (~4) when copper is heated from room temperature to its 1356°K melting point than that required ($\geq$20) to produce the substantial reflectance drop to Fig. 1-type plateau values.

Finally, it is clear from the plots of n and ν_c in Figure 6 that even with the improved input data listed in Table I, the theory of Ujihara does not have the correct functional dependence with temperature for either the index of refraction or the electron-phonon collision frequency for T<500°K. Refinements such as a departure from sphericity of the Fermi surface and more than one electron-phonon collision frequency could be considered to improve the Ujihara treatment.

Reflectance Measurements

Other explanations for the reflectance behavior which is shown in Figure 1 fall into three categories: (1) a surface deformation which directs the reflected beam away from the detector, (2) plasma formation which absorbs or scatters the reflected light, or (3) a nonlinear process causing enhanced absorption within the metal. The first two categories involve processes which produce a reduction in light reaching the detector that could be misinterpreted as a decrease in the reflectance of the solid target surface. The importance of the first category, surface deformation, may be evaluated by comparing specular reflectance with total reflectance. The initial experiments of Bonch-Bruevich

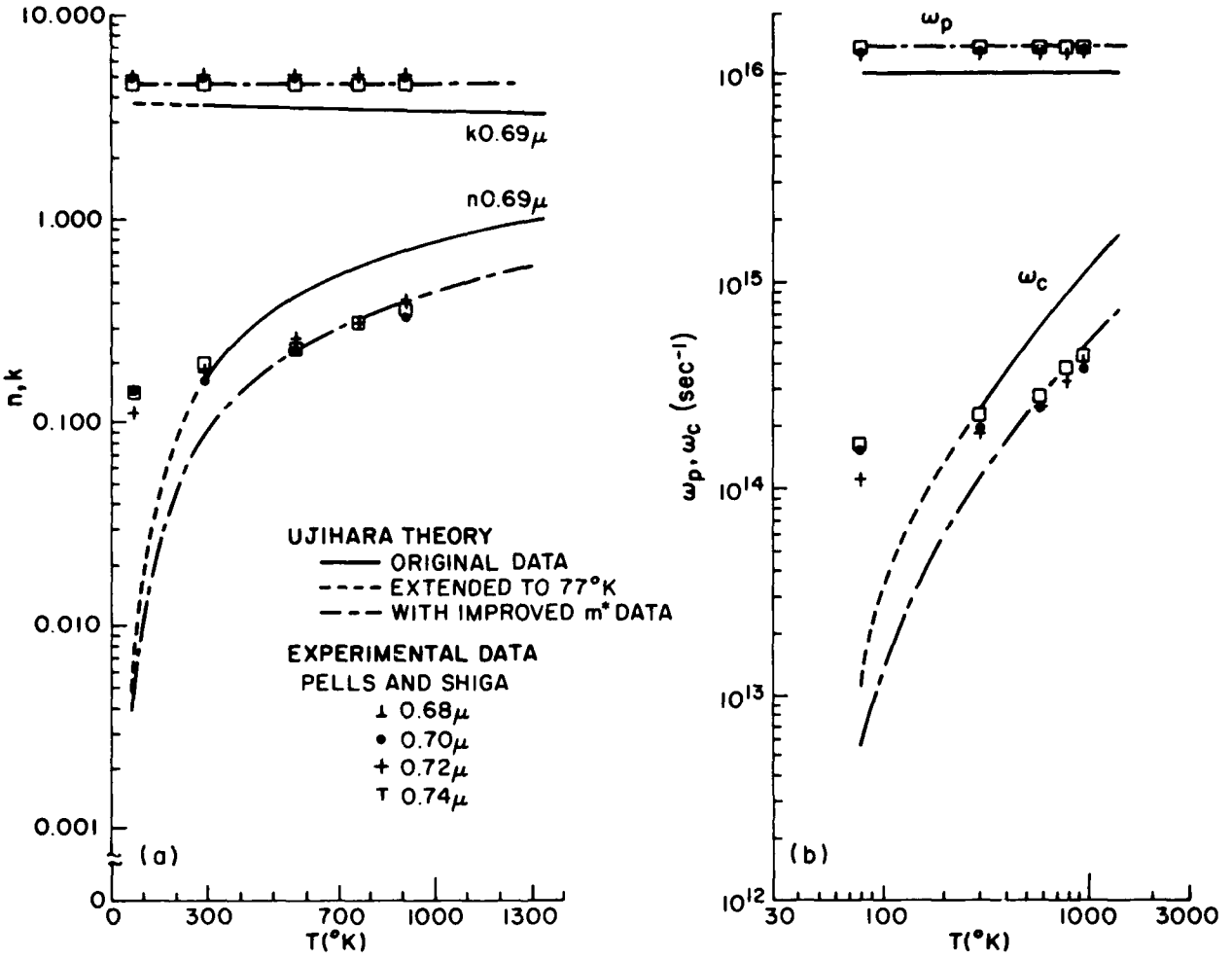

Fig. 6 - Temperature Dependence in Copper of (a) Optical Material Properties: index of refraction n and extinction coefficient k and (b) Free-Electron Material Properties: plasma frequency ω_p and electron-phonon collision frequency ν_c.

(Figure 1a) apparently measured total reflectance while those of Zavecz (Figure 1c) were specular reflectance measurements.

Experimentally, the reflectance of the metal surface is obtained by dividing the reflected pulse by the incident laser pulse. For a 30-ns laser pulse, even a time registration error as small as 1 ns between these two pulses can cause a significant error in the measured reflectance. This is indicated in Figure 7 where the solid pulse curve represents 30-ns FWHM Gaussian incident and reflected pulses, and the solid horizontal line is the corresponding reflectance. Time registration errors of 1 and 3 ns are shown by the dashed curves with the dashed reflected pulses now preceding the solid incident laser pulse curve. A shift of only 1 ns, corresponding to 3% of the width, can cause a reflectance error of as high as 25% in the wings of the pulse shape.

To avoid a time registration error, Park and Walter[11] used a single detector for both pulses and sent the sample of the incident laser pulse through an air delay path. They carried out both specular and total reflectance measurements on copper targets. The experimental arrangement is sketched in Figure 8. A TRG model 104 ruby laser operating in the Q-switched mode produced 0.6J in a 30-ns FWHM pulse. A one to four beam expander

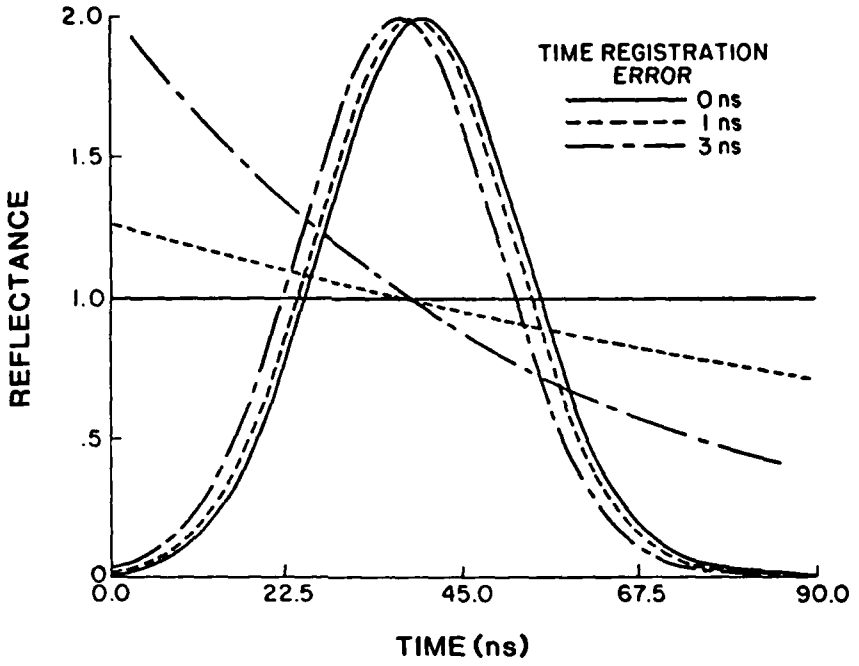

Fig. 7 - Computed Reflectance for 30-ns FWHM Gaussian reflected and incident laser pulses with 0, 1, and 3-ns time registration errors.

reduced the measured beam divergence to ≃1 mrad. A high intensity beamsplitter provided a sample of the incident pulse which was delayed through an air path of ≃20m for specular reflectance measurements and ≃50m for total reflectance measurements. The targets were located in a vacuum chamber, and a mechanical pump reduced the chamber pressure below 0.1 Torr to avoid air breakdown at the target surface.

The copper target surfaces were produced by vacuum-deposition on a glass plate of good optical quality. Electroplating was used to back up the ≃2000 Å thick copper film on the glass plate and produce a mechanically-strong copper target a few mm thick. Just before the reflectance measurements were made, the vacuum-deposited target was removed from the glass plate and placed in the vacuum chamber. In this way an optical-quality copper surface could be prepared and protected until the measurements were taken.

At the focused spot ≃0.5-mm diam on the copper target, a maximum intensity of $10^9 W/cm^2$ was produced. This was determined from a measured energy of 75mJ at the target location. Corning glass filters were used as attenuators. For the total reflectance measurements indicated in Figure 8b, an integrating sphere consisting of two plastic hemispheres coated with Eastman White Reflectance coating (barium sulphate) was placed in the vacuum chamber. Not only does an integrating sphere carry out a spatial integration of all light reflected from the target surface, but it delays the arrival of the light at the detector by varying times depending on the path within the sphere. The 30-ns FWHM ruby laser pulse was lengthened by ≃10 ns when detected by a fast vacuum photodiode located at the top of the sphere. Because of the pulse-lengthening property of the integrating sphere, a longer air delay path, ≃50m, was required to avoid overlapping the reflected and sample laser pulses. As indicated in Figure 8b, the sample of the incident laser pulse was directed through a second entrance window into the integrating sphere, but was not focused on the surface of the sphere.

For each reflectance measurement, a Polaroid picture was taken of the Tektronix 519 oscilloscope trace and enlarged as shown in Figure 9 for digitization of the reflected and sample pulse shapes into a PDP 11 minicomputer.

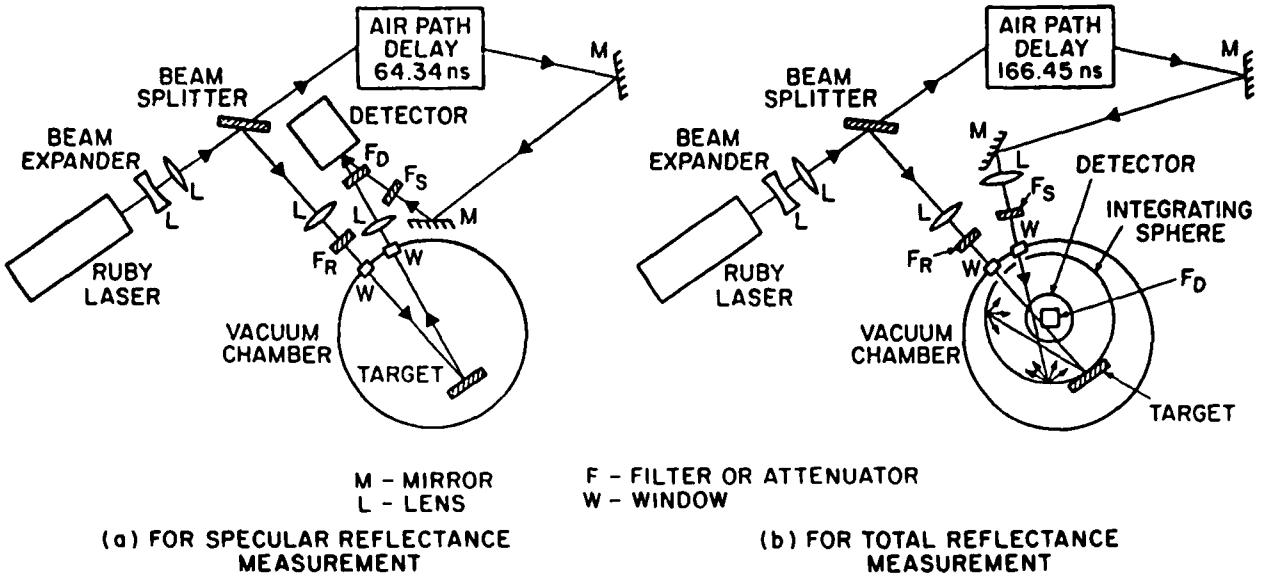

Fig. 8 - Experimental arrangement.

Computer programs were developed to remove the air-path time delay, insert the transmittances and reflectances of optical elements and then calculate and display the reflectance behavior during the laser pulse. Park and Walter's specular and total reflectance results[11] are shown in Figures 10 and 11 for three incident laser power densities, ~2, 5 and 9×10^8 watts/cm^2. The curves shown are a normalized incident laser pulse, the reflected pulse and the metal target's reflectance behavior which is the ratio of the two pulse curves. The laser energy absorbed was calculated from these results and the temperature history of the metal surface determined using a one-dimensional heat-conduction approach.

The measured total reflectances of evaporated-copper target surfaces show a slow decrease with increasing incident laser intensity or increasing surface temperature up to the boiling point of the metal. At low incident laser power densities (i.e., $<3 \times 10^8$ W/cm^2) the specular and total reflectances of the metal target surface are similar (cf. Figure 10a with Figure 11a). The one-dimensional heat-conduction calculations indicate that the

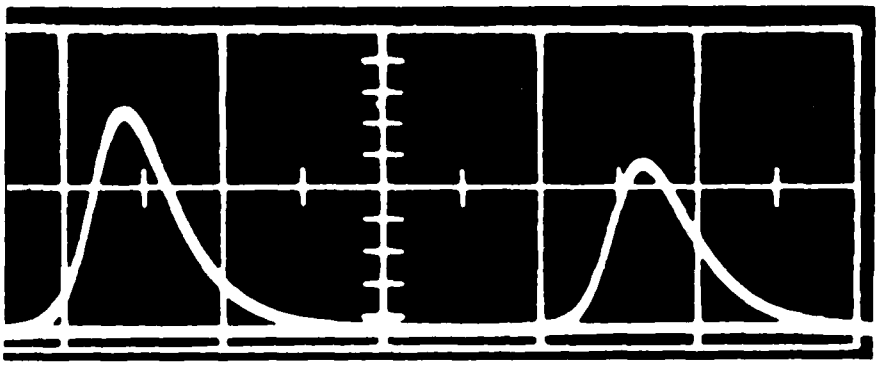

Fig. 9 - Enlargement of an oscilloscope trace showing the specularly-reflected pulse from an evaporated-copper target surface and a sample of the incident 3.15×10^8 W/cm^2 ruby laser pulse. The horizontal time scale is 50 ns/large division.

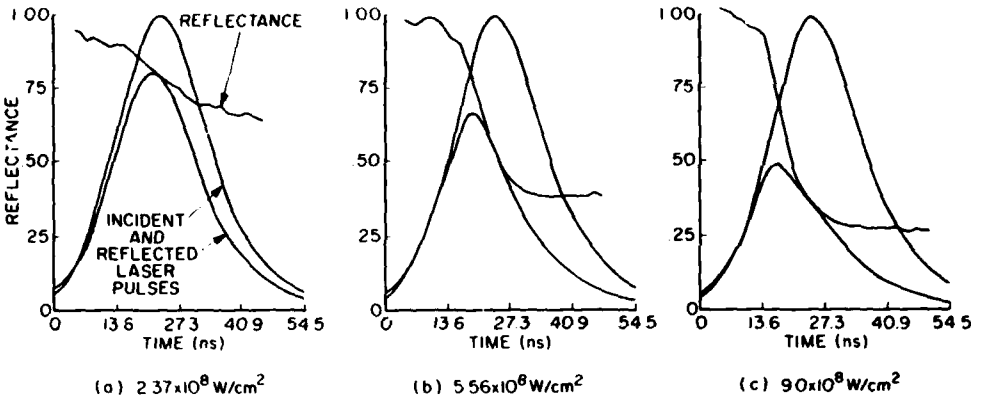

Fig. 10 - Specular Reflectance of Copper.

copper surface did not reach its melting point with this incident laser power density; namely, $2 \times 10^8 W/cm^2$. No permanent damage was observed in the copper. The copper target was examined under 200x magnification and no trace of melting was observed. The lack of any permanent observable damage is consistent with the calculated maximum surface temperature of $1040^{\circ}K$ and with the equality of the specular and total reflectances.

At an incident laser power density of $5.6 \times 10^8 W/cm^2$, the specular reflectance undergoes a sharp drop which is not observed in the total reflectance (cf. Figure 10b with Figure 11b). The one-dimensional heat-conduction calculation indicates that the maximum temperature attained by the copper surface was in excess of the boiling point. Permanent damage was observed at the interaction site. Once again the permanent changes observed in the target are consistent with the surface temperatures calculated and the reflectances measured which reveal a decrease in the specular accompanied by an increase in the diffuse component of the reflectance.

An additional increase in incident laser power density to $7.9 \times 10^8 W/cm^2$ continues the decrease in specular reflectance (Figure 10c compared with 10b). Permanent target surface damage is more severe and the crater site is more extensive. The recovery in the total reflectance behavior which is evident in Figure 11c is caused by a "light flash" produced by emission of light from a plasma that is formed at or in front of the metal surface. The spectral content of this light includes sharp emission lines from neutral copper atoms, copper ions and copper dimers (Cu_2 molecules) as indicated in Figure 12. These sharp emission features are superimposed upon a continous background. They were recorded on Polaroid film using a 0.5m Jarrell-Ash Ebert spectrometer. Our current research program

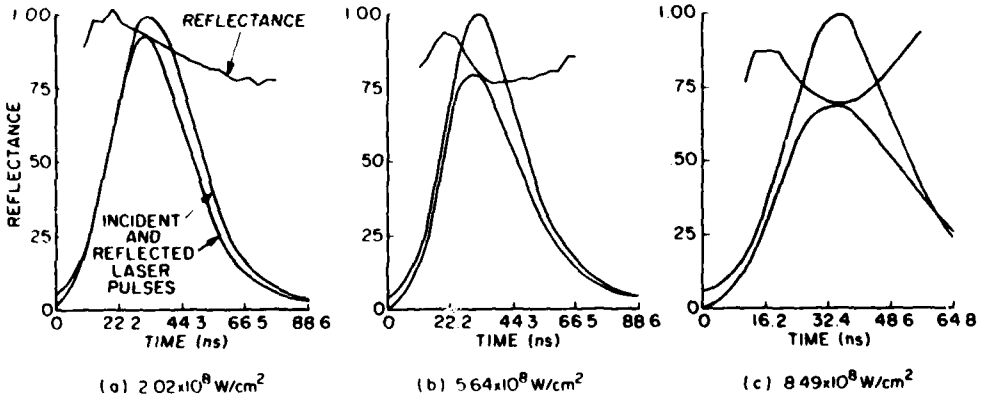

Fig. 11 - Total Reflectance of Copper.

includes improvement of the spectral resolution to identify the type and state of excitation of the emitting species. Temporal resolution is also being used to identify the order in which the different species are excited and contribute to the "light flash."

When an interference filter is inserted in front of the TRG 105B vacuum photodiode thereby restricting the light detected to ±50 Å around the 6943 Å ruby laser wavelength, then the recovery in total reflectance behavior so evident in Figure 11c and just noticeable in Figure 11b disappears. Our most recent reflectance behavior results are shown in Figure 13 for three different surface preparations of the copper target: vacuum-deposited, diamond-turned and mechanically-polished polycrystalline. These results were obtained with a ruby-laser interference filter included in the detection system. Notice that we are begining to see differences in the reflectance behavior for different surface preparations. This provides some preliminary confirmation for the monitoring of optical properties of target materials to identify the relevant processes taking place during the laser-material interaction.

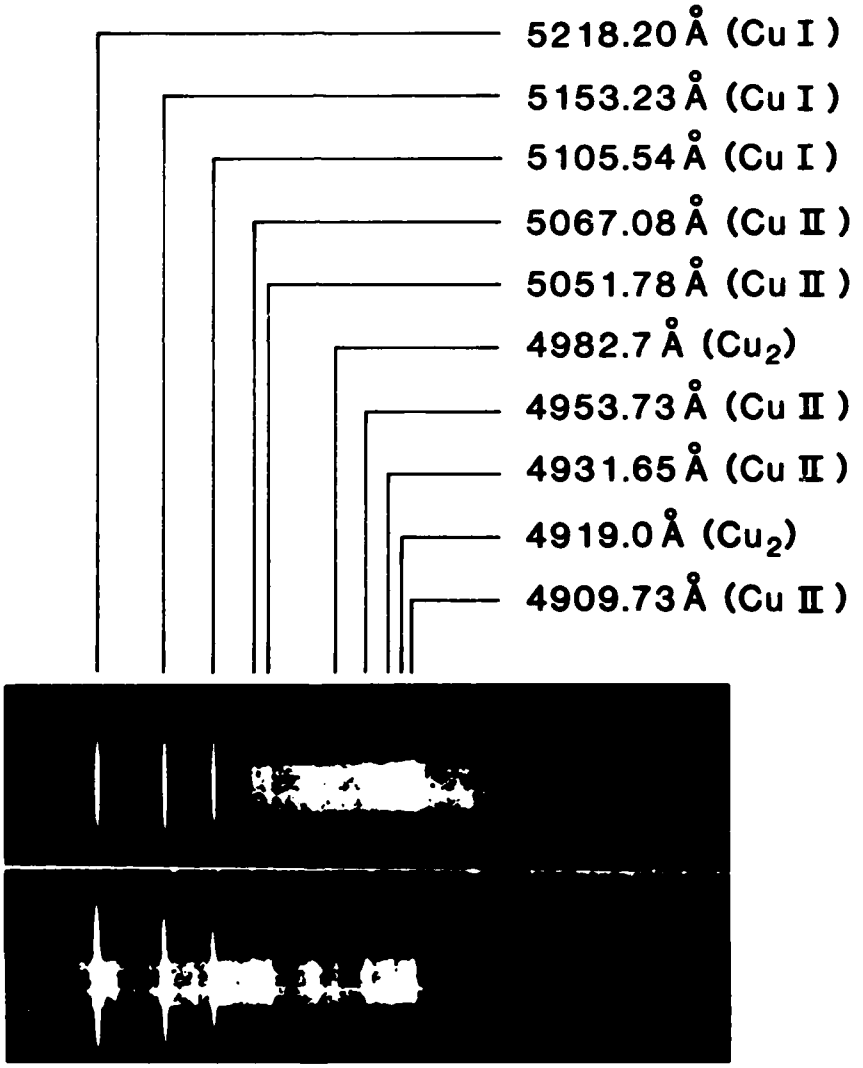

Fig. 12 - Spectral Characteristics of the "Light Flash" in the blue-green region.

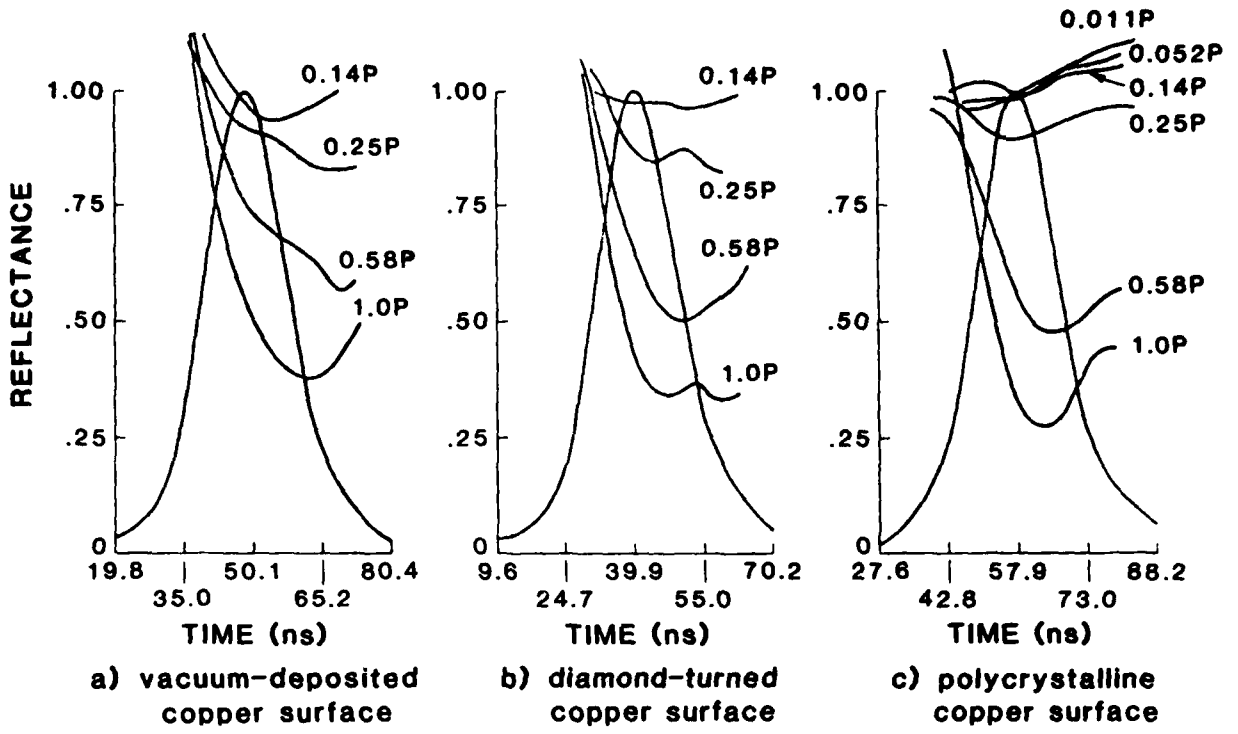

Fig. 13 - Total Reflectance Behavior for different copper surface preparations. P corresponds to an incident ruby laser power density of 1.5×10^9 W/cm^2.

Conclusions

Surface deformation and plasma formation have been observed by means of direct real-time measurements of the target material's optical properties with nanosecond resolution. Thus far we may conclude that specular reflectance is a sensitive indicator of surface deformation. Total reflectance measurements, on the other hand, indicate that until the surface temperature of a metal target reaches the vicinity of the boiling point, the total reflectance does not differ significantly from that given by a Drude-type free-electron model. These results are in agreement with those of von Allmen et al.[9] but contradict the conclusion of others that a decrease of ≥50% in the total reflectance occurs at or possibly even before the melting point of a metal surface is reached. Spectral emission lines have been observed from neutral atoms, ions and dimers in the plasma formed as the surface temperature of copper exceeds the boiling point.

Acknowledgements

This research has been supported in part by the Office of Naval Research under Contract No. N00014-78-C-0678. The helpful collaboration of N. Marcuvitz and M. Newstein, measurement assistance of W. Woturski and R. DiFazio, target preparation by M. Eschwei and S. Bielaczy, and computer programming by F. Richter and P. Levin are gratefully acknowledged.

References

1. A. M. Bonch-Bruevich, Ya. A. Imas, G. S. Romanov, M. N. Liebson and L. N. Mal'tsev, "Effect of a Laser Pulse on the Reflecting Power of a Metal," Sov. Phys.-Tech Phys. 13, 640-643 (1968).

2. N. G. Basov, V. A. Boiko, O. N. Krokhin, O. G. Semenov and G. V. Sklizkov, "Reduction of Reflection Coefficient for Intense Laser Radiation on Solid Surfaces," Sov. Phys.-Tech. Phys. 13, 1581-1582 (1969).

3. A. M. Prokhorov, V. A. Batanov, F. V. Bunkin and V. B. Federov, "Metal Evaporation under Powerful Optical Radiation," IEEE J. Quantum Electronics QE-9, 503-510 (1973).

4. T. E. Zavecz, M. A. Saifi and M. Notis, "Metal Reflectivity under High-Intensity Optical Radiation," Appl. Phys. Lett. 26, 165-168 (1975).

5. J. C. Koo and R. E. Slusher, "Diffraction from Laser-Induced Deformation on Reflective Surfaces," Appl. Phys. Lett. 28, 614-616 (1976).

6. J. F. Ready, "Change of Reflectivity of Metallic Surfaces During Irradiation by CO_2-TEA Laser Pulses," IEEE J. Quantum Electronics QE-12, 137-142 (1976).

7. P. W. Chan, Y. W. Chan and H. S. Ng, "Reflectivity of Metals at High Temperatures Heated by Pulsed Laser," Phys. Lett. 61A, 151-153 (1977).

8. Yu. I. Dymshits, "Reflection of Intense Radiation from a Thin Metal Film," Sov. Phys.-Tech. Phys. 22, 901-902 (1977).

9. M. von Allmen, P. Blaser, K. Affolter and E. Sturmer, "Absorption Phenomena in Metal Drilling with Nd-Lasers," IEEE J. Quantum Electronics QE-14, 85-88 (1978).

10. C. T. Walters and A. H. Clauer, "Transient Reflectivity Behavior of Pure Aluminum at 10.6μm," Appl. Phys. Lett. 33, 713-715 (1978).

11. K. Park and W. T. Walter, "Reflectance Change of a Copper Surface During Intense Laser Irradiation," pp. 274-282 in Proceedings of the International Conference on LASERS '78, V. J. Corcoran, ed.; Orlando, Florida, December 1978, and "Metal Reflectance Changes During Intense Laser Irradiation," pp. 21-31 in Applications of Lasers in Materials Processing, E. A. Metzbower, ed.; American Society for Metals, Metals Park, Ohio, 1979.

12. N. F. Mott and H. Jones, The Theory of the Properties of Metals and Alloys, Clarendon Press, Oxford, England (1936).

13. K. Ujihara, "Reflectivity of Metals at High Temperature," J. Appl. Phys. 43, 2376-2383 (1972).

14. N. F. Mott and H. Jones, op cit p. 116.

15. G. Hass et al., 1965, as quoted in American Institute of Physics Handbook, D. E. Gray, ed.; McGraw Hill, New York pp. 6-157 (1972).

16. N. F. Mott and H. Jones, op cit p. 278.

17. W. T. Walter, "Reflectance Changes of Metals During Laser Irradiation," in Laser Applications in Materials Processing, J. F. Ready and C. B. Shaw, Jr., ed.; Proc. of SPIE 198, 109-117 (1980).

18. K. Forsterling and V. Freedericksz, Ann. Physik 40, p. 200 (1913), as quoted in M. P. Givens, "Optical Properties of Metals," p. 324 in Solid State Physics 6 Academic Press, New York (1958).

19. G. P. Pells and M. Shiga, "The Optical Properties of Copper and Gold as a Function of Temperature," J. Phys, C. (Solid St. Phys.) 2, 1835-1846 (1969); and G. P. Pells, n and k data furnished by private correspondence as indicated in this reference.

20. L. G. Schulz, "An Experimental Confirmation of the Drude Free Electron Theory of the Optical Properties of Metals for Silver, Gold and Copper in the Near Infrared," J. Opt. Soc. Am. 44, 540-545 (1954).

21. K. Weiss, Z. Naturforsch 3a, 143 (1948), as quoted in American Institute of Physics Handbook, D. E. Gray, ed.; McGraw Hill, New York pp. 6-133 (1972).

22. S. Roberts, Phys. Rev. 118, 1509 (1960), as quoted in American Institute of Physics Handbook, D. E. Gray, ed.; McGraw Hill, New York pp. 6-133 (1972).

23. F. P. Gagliano and V. J. Zaleckas, "Laser Processing Fundamentals," in Lasers in Industry, S. S. Charschan, ed.; Van Nostrand Reinhold, New York p. 146 (1972).

SHOCK DEFORMATION AND MICROSTRUCTURAL EFFECTS ASSOCIATED WITH PULSE LASER-INDUCED DAMAGE IN METALS

by

K. MUKHERJEE

T. H. KIM

W. T. WALTER

Reprinted from:

LASERS IN METALLURGY

Proceedings of a symposium sponsored by the Physical Metallurgy and Solidification Committees of The Metallurgical Society of AIME, held at the 110th AIME Annual Meeting, Chicago, Illinois, February 22-26, 1981.

Edited by
K. MUKHERJEE
Michigan State University
East Lansing, Michigan 48824
and
J. MAZUMDER
University of Illinois at
Urbana-Champaign
Urbana, Illinois 61801

CONFERENCE PROCEEDINGS

The Metallurgical Society of AIME

SHOCK DEFORMATION AND MICROSTRUCTURAL EFFECTS

ASSOCIATED WITH PULSE LASER-INDUCED DAMAGE IN METALS*

K. Mukherjee
Michigan State University
East Lansing, MI 48824

T. H. Kim
&
W. T. Walter
Polytechnic Institute of New York
New York, NY 11201

Shock deformation and microstructural effects associated with pulse laser interaction with metallic surfaces, are reviewed. Some recent results of laser damage in low melting point metals are reported. A wavy deformation pattern in these metals is associated with a decaying elastic wave propagation through an elastically inhomogeneous medium. Defect structures and void formation in vapor deposited pure Cu are reported and discussed.

* This work was partially supported by the U. S. Office of Naval Research.

Introduction

It is now well known that stress waves and associated shock deformation of solid targets can be produced with Q-switched laser pulses (1-19). Highly localized thermal expansion, in the wake of a rapid laser pulse at the surface of an elastic solid, promotes a stress wave which then propagates into the interior of the solid. The magnitude of the peak stress becomes appreciable as the pulse duration becomes shorter. If the duration of the pulse is such that the stored elastic distortional energy is greater than or equal to that necessary for yielding, then plastic deformation will occur.

The initial impact of the laser energy pulse is analogous to a high strain rate explosive shock wave deformation of the material (12). In fact, a striking similarily between the defect structure and deformation, produced by explosive shock loading and Q-switched laser pulse damage has been reported (19). In unconfined thin metal foils (250Å to 1 μm thick) a peak stress of the order of 1 k. bar has been reported for 25 to 50 n. sec duration Q-switched pulses (11). An order of magnitude higher peak stress for the same materials was observed with a plasma confining transparent overlay (11). In a similar experiment with vapor deposited confined thin foils (1 μm to 10 μm) of various pure elements (B, C, Mg, Al, Si, Ti, Cr, Mn, Fe, Co, Ni, Cu, Zr, Mo, Ag, In, Sb, Pt, Au, Pb, and Bi), it was found that the peak stress is approximately a linear function of the laser energy fluence (12). Peak pressures as high as 250 k. bars have been estimated for W and Mo wires by comparing vacancy concentration produced by a Q-switched ruby laser (35 J/cm^2 fluence) and that produced by explosive shock loading (19).

The stress wave generated by a laser pulse can give rise to elastic and plastic deformation, formation and rearrangement of dislocations, formation of vacancies and formation of vacancy clusters leading to microporosity etc. The above mentioned effects are important from the metallurgical point of view since these can alter microstructure and mechanical properties of metals and alloys. Beyond a threshold energy density, for a given material, melting and crater formation, sputtering and plasmaformation are possible (17,18,20-28). If melting is involved, then subsequent ultra rapid solidification can produce metallic glasses, ultrafine grain structure, metastable phases and a very large concentration of vacancies (19,29-34).

Coupling of the incident laser light with the metallic target, on the other hand, can be influenced by inherent structural discontinuities such as vacancies, dislocations, grain boundaries and inclusions. A better understanding of the laser-materials interaction and the role of various structural singularities in this interaction, is essential for a more efficient application of lasers in materials processing. In this paper, shock wave phenomenon and microstructural aspects associated with pulse laser interaction with metals are briefly reviewed and some new results related to these effects are presented.

Mechanism of Shock Wave Formation

Several mechanisms of laser induced shock wave formation can be postulated. The laser photon energy is almost instantaneously absorbed on the metal surface as thermal energy, producing a highly localized temperature excursion. If the local temperature reaches or exceeds the boiling point of the metal then a rapid vaporization occurs. The recoil pressure of the

escaping (vapor) atoms (without ionization) could possibly set up the shock deformation in that case. If the laser energy fluence is high enough to produce a plasma, then the expanding plasma can also provide the shock wave. But shock phenomenon and/or plastic deformation have been reported for laser energy fluences less than that for melting (18). In such a case, the thermal stress must be the predominant cause. Of these, the thermal stress and plasma effects appear to be the two important modes as far as current experimental results are concerned.

Thermal Effects

Heating by Q-switch laser pulses is nearly approximated by a constant volume process. As the laser energy is absorbed in a thin surface layer, the internal energy of the irradiated volume of material increases. If the rate of heating of this volume is very rapid, as in the case of a Q-switched pulse, then the normal thermal expansion of this volume can not take place because of the inability of the adjacent matrix to relax at a rate commensurate with the temperature rise. Thus a pressure wave in the form of a compressive shock wave is produced, which travels through the material.

The amplitude of the elastic wave, produced for a given absorbed laser energy fluence, depends on the elastic constraints applied at the heated surface. If the heated surface is free (stress-free), the wave amplitude could be relatively small compared with that for a constrained surface (such as a transparent overlay). The nature of this thermo elastic stress can be examined by considering a homogeneous isotropic solid as follows (2).

Let us consider a semi-infinite surface with a localized transient heat source as shown in Figure 1.

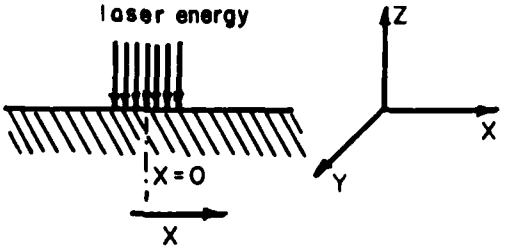

Fig. 1 - Transient, symmetric and uniform heat source.

For simplicity, it is assumed that heat is absorbed at the surface $Z = 0$ and the laser energy is uniform across the spot diameter. In reality, however, the energy distribution within the spot is ~ gausian and the heat energy will be deposited in a layer of thickness δ, given by the skin depth for the electromagnetic radiation:

$$\delta = c/\omega\,|\varepsilon|^{\frac{1}{2}} \qquad (1)$$

where c and ω are the velocity and angular frequency of the laser light and ε is the real part of the dielectric constant of the metal.

As a result of this surface heat absorption there is a surface temperature rise and an associated elastic strain. At this point we consider an

one-dimensional problem, i.e., $e_{xx} = e_{yy} = 0$, since we have seen that the rigidity of the surrounding matrix during a Q-switched laser heating does not allow the lateral volume expansion. The only non zero strain e_{zz} is then:

$$e_{zz} = \frac{\partial u(z,t)}{\partial z} = \alpha \Delta T(z,t) \tag{2}$$

where u(z,t) is the z-component of particle displacement, α is the coefficient of linear thermal expansion and $\Delta T(z,t)$ is the temperature rise. If the strain, $e_{zz} = \alpha \Delta T$, was produced by a stress σ_{zz} without the temperature rise, then $\sigma_{zz} = -Be_{zz} = -B\alpha\Delta T$, where B is the bulk modulus of the metal. In the presence of both heating and actual stress, then (35)

$$\sigma_{zz} = (\lambda + 2\mu)\, e_{zz} - B\alpha\Delta T \tag{3}$$

where λ and μ are the first Lamé constant and the modulus of rigidity respectively. The equation of motion for the particle displacement is thus given by:

$$\rho \left(\frac{\partial^2 u}{\partial t^2}\right) = \left(\frac{\partial \sigma_{zz}}{\partial z}\right) = (\lambda + 2\mu) \left(\frac{\partial^2 u}{\partial t^2}\right) - B\alpha \left(\frac{\partial \Delta T}{\partial z}\right) \tag{4}$$

where ρ is the density of the metal. Utilizing the relationship

$$(\lambda + 2\mu) = \rho v^2 \tag{5}$$

where v is the velocity of elastic wave propagation in the metal, we can write

$$\frac{1}{v^2} \left(\frac{\partial^2 u}{\partial t^2}\right) = \left(\frac{\partial^2 u}{\partial z^2}\right) - \frac{B\alpha}{\rho v^2} \left(\frac{\partial \Delta T}{\partial z}\right) \tag{6}$$

A formal solution of equation (6) requires an actual temperature distribution function $\Delta T(z,t)$, and the solution involves evaluation of rather cumbersome integrals. A qualitative picture of the functional dependence of the stress-wave amplitude on the elastic properties of metal can, however, be obtained by numerical solutions after substitution of an empirical (12) exponential form of the temperature distribution function, $\Delta T(z,t)$.

Once, this elastic deformation is initiated, four different types of elastic waves propogate in the solid (11). The leading wave is an elastic dilatational wave. As this dilatational wave sweeps across the surface, a series of waves is generated. Using Huygens principle, an envelop of these waves can be defined and this envelop is called the Von Schmidt wave. The dilatational wave is followed by a shear wave with a velocity $v_s < v_e$ where v_e is the elastic wave velocity. A Rayleigh wave is also produced on the surface with a velocity $v_R < v_s$. Plastic deformation will occur if the distortional elastic energy in these waves exceeds that necessary for yielding. The qualitative nature of various elastic waves are shown in Figure 2.

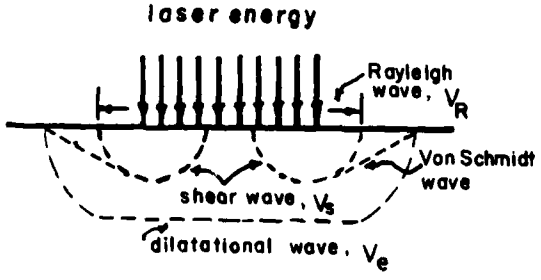

Fig. 2 - Elastic wave system induced by an uniform laser pulse source.

Plasma Effects

At a laser energy density above the threshold for melting and evaporation a hot plasma can form. The expanding plasma can induce a shock wave in the material. We are, however, considering the laser interaction with metals in vacuum. Thus the possibility of a LSD-wave proproduced in air, which can also induce a shock wave, is not discussed.

The essential difference between the thermoelastic shock wave as discussed earlier and the plasma induced shock wave is that the latter is more nearly a surface stress source than the former. Thus the boundary constraint in the plasma induced shock deformation is different from those in the thermo-elastic case. Further more, confinement of plasma, with an overlay, will have a much more pronounce effect on the shock intensity. In fact, experimental results indicate that the peak pressure can be at least an order of magnitude larger if the plasma is confined.

Experiments which measured momentum transfer to various target metals as a function of laser intensity, show an optimum intensity for each metal (36) as shown schematically in Figure 3.

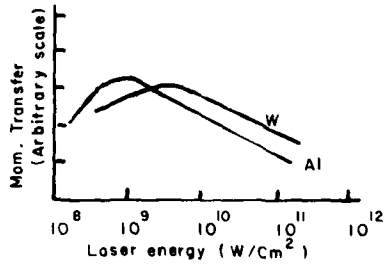

Fig. 3 - Momentum transfer as a function of laser energy density.

An explanation of the behavior, as shown in Figure 3, is that below the optimum energy, some energy is lost by thermal conduction and above the maximum, some energy goes in increasing ionization and temperature of the plasma. Thus it will appear that for a given material, the plasma induced shock pressure will decrease with increasing laser energy density beyond the optimum value.

Nature of Shock Deformation

Thin Films

In stainless steel and in 6061-T6 Al foils (0.4 to 0.6 mm thick), the permanent deformation mode is found to be independent of the confinement, although the peak pressure pulse was measured to be an order of magnitude higher for the confined samples (11). The rise time of the pressure pulse, for the unconfined samples in this experiment, was found to be comparable to the laser pulse rise time; 25-30 n. sec. In the confined samples, both the pressure pulse rise time and pulse decay were considerably longer.

Shock wave peak-pressure pulse measurements have been reported for a large number of pure element foils, 1 μm to 10 μm thick at energy fluences up to 12J/cm^2. These samples were confined between glass plates and a 15 n. sec. duration Q-switched ruby laser pulse was used. It was found that the peak shock pressure is approximately a linear function of laser fluence (12).

Bulk Samples

It has been reported (13) that in confined pure Fe samples, the peak shock pressure increases with the reduction in sample thickness at an energy density of 4^{9} , c^{2} and a pulse duration of 20-80 n. sec. For example a peak pressure of 39.6 k. bar was observed for a 14 μm thick compared with a peak pressure of 9.2 k. bars for a 3 mm thick sample. Most importantly, the rise-time of the pressure pulse is comparable to the rise-time of the laser pulse in both cases. However, the decay time of the pressure pulse is much longer than the laser pulse in the thicker samples. A qualitative nature of the pressure pulse shape as a function of sample thickness is shown in Figure 4.

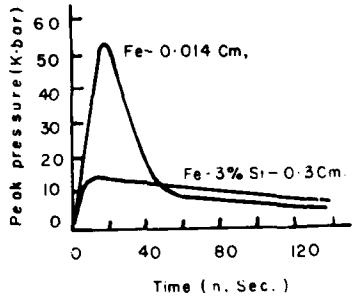

Fig. . - Pressure-pulse ... as a function of specimen thickness (13).

Slip, deformation and surface markings produced by the shock wave have been studied by several investigators (10,15-19,37-41). Both polycrystalline and single crystal metallic surface show crystallographic slip (10, ...-19) as well as slip and periodic ripple patterns (16,37) induced by high energy pulse laser. In semiconductor materials, a highly periodic ripple pattern is also reported. In a single crystal Si sample, a 30 n. sec. Q-switched ruby pulse, 10^{8} w/cm^2, produced twinned structures on (111) planes.

In single crystals of Cu and Al, multi threshold damage studies have been reported (17,18). Intragranular crystallographic slip and grain boundary sliding in polycrystalline Cu and Al are observed at laser energies well below the threshold for melting (17,18). These authors have also reported that the existing imperfections such as dislocations, grain boundries etc., lower the threshold for melting and other catastropic damage, but increases the threshold for plastic deformation. These results are indeed important in terms of understanding the mechanism(s) of coupling of pulse laser energy on metal surfaces and for the consideration of pulse laser applications in materials and metals processing. One interesting observation (18) is that a symmetric six-fold slip pattern on the (111) surface of Cu single crystals is observed at laser fluences up to the threshold for plasma formation. The six-fold pattern is replaced by a 3-fold pattern at intensities which produce a hot plasma. The six-fold slip pattern therefore, is associated with the thermoelastic shock wave and the 3-fold pattern, perhaps is related to a different boundary constraint situation associated with the plasma shock wave as discussed earlier. The nature of crystallographic slip on various orientations of Al single crystals are also reported in the literature for $\sim$ 100 n.s. duration pulse envelope from a CO_2-TEA laser at energies $\sim$ 37J/cm^2.

Spallation and Fracture

Photographic evidence of back face spallation of 1.0 mm thick 6061-T6 Al alloy has been reported (19). These samples were irradiated in vacuum with 1.06 m, sec., 1.06 μ laser pulses at fluences as high as 8600 J/cm^2. It is also reported by this author that low-energy pre-pulsing lowered the subsequent spallation threshold. It is believed that the prepulsing improves the coupling of the laser energy with the metal surface.

Non Equilibrium Vacancy Concentration

From field-ion microscopy studies, Murr et al. (42,43) have demonstrated that vacancy and vacancy clusters are produced in explosively shock-loaded Mo. In a later experiment, field-ion microscopy was performed [illegible] laser irradiated [illegible]. The results of increasing vacancy concentration with increasing laser fluence can be compared with similar observations in the explosively shock loaded Mo and W. At a laser fluence of 35J/cm^2 a vacancy concentration as high at 6 at . was recorded for Mo and a vacancy concentration of 0.9 at.percent was observed for W at a laser fluence of 29J/cm^2. A direct comparison of vacancy concentration produced by an explosive shock and a laser pulse, led these authors to estimate a peak pressure pulse [illegible] kbars at the maximum laser fluence.

We have observed [illegible] produced in vapor deposited Cu foils irradiated with [illegible] pulses, $\sim 10^9$ w/cm^2 and 20 n. sec. FWHM. These results will be presented later.

[illegible] Mechanisms

Recently (19), dislocation etch pit studies have been performed on (111) planes of high purity single crystal Cu. This study shows a symmetric six-fold etch-pit pattern around the pulse laser damage spot as shown schematically in figure [illegible].

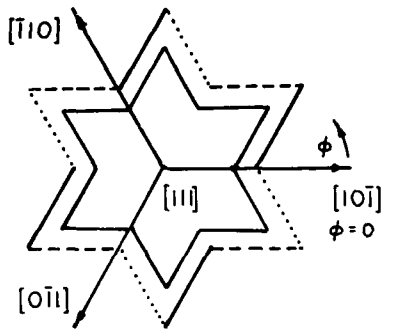

Fig. 5 - Schematic presentation of etch-pits on the (111) surface of a Cu single crystal.

There are nine different orientations of edge dislocations and three screw dislocations which intersect the (111) surface and therefore, may lead to etch pit formation. The force F on a dislocation line l and Burgers vector b is given by $F = \sigma b \times L$. In the case of a thermoelastic stress, generated by a circular surface source, σ is a tensor. These authors assumed a stress field, in a cylindrical co-ordinate system (origin of the co-ordinate system is in the center of the laser spot of radius R) as follows:

$$\sigma_{rr} = -\frac{1}{2} E.\beta.\Delta T \left(\frac{R}{r}\right)^2 \qquad \text{for } r > R$$

$$\sigma_{\phi\phi} = +\frac{1}{2} E.\beta.\Delta T \left(\frac{R}{r}\right)^2 \qquad \text{for } r > R \qquad (7)$$

$$\sigma_{rz} = \sigma_{zz} = 0$$

A calculation of forces on the twelve orientations of the dislocations using the stress field shown in equation (7), shows that the largest forces act on the three edge dislocations shown in Table 1.

Table 1. The Nature of Dislocations on Which Maximum Force Acts

Dislocation	Direction of b	Direction of L	Slip Plane	Slip Trace ∥ to
D_1	$1\,0\,\bar{1}$	$\bar{1}\,\bar{2}\,\bar{1}$	$\bar{1}\,1\,\bar{1}$	$1\,0\,\bar{1}$
D_2	$0\,\bar{1}\,1$	$\bar{2}\,\bar{1}\,\bar{1}$	$1\,\bar{1}\,\bar{1}$	$0\,\bar{1}\,1$
D_3	$\bar{1}\,1\,0$	$\bar{1}\,\bar{1}\,\bar{2}$	$\bar{1}\,\bar{1}\,1$	$\bar{1}\,1\,0$

The magnitudes of the forces on these dislocations D_1, D_2 and D_3 respectively have maximum for angles (note $\phi = 0$ for $[10\bar{1}]$ direction and $Z = 0$ on the (111) plane) as follows:

$$\phi_1 = 45^\circ + n.\ 90^\circ$$
$$\phi_2 = 15^\circ + n.\ 90^\circ \qquad n = 0,1,2,3 \qquad (8)$$
$$\phi_3 = 75^\circ + n.\ 90^\circ$$

If we draw the traces of only those slip systems for which the acting forces are largest, then a parallel pattern at an angular interval $\Delta\phi = 30^\circ$, as shown in Figure 5 is obtained and it matches exactly with the experimental etch pit pattern.

Deformation Modes in Low Melting Point Metals

We have investigated crater and plasma formation and shock deformation in several high purity metals including low melting point Sn, Zn and Bi polycrystals. A Q-switched ruby laser with a pulse duration ~ 20 n. sec. and energy densities up to ~ 1.5×10^9 w./cm^2 was used for these experiments and samples were irradiated in vacuum. Figure 6, shows a scanning electron microstructure of the laser damaged crater as well as the adjacent surface in Sn at a fluence ~ 1.5×10^9 w/cm^2.

Fig. 6 - Wavy deformation pattern in Sn. Scanning electron micrograph. Fluence ~ 1.5×10^9 watts/cm^2.

A wavy surface deformation pattern is observed in this figure. Several points to be noted with reference to this observation: (a) the amplitude of the wavy deformation is maximum near the crater edge, (b) the amplitude of the wavy deformation decays with increasing radial distance r from the center of the crater, (c) the spacing of the ripples (wave length) decreases as r increases and (d) distortion and pinning of the wave front at grain boundries. The nature of this wavy deformation is schematically presented in Figure 7.

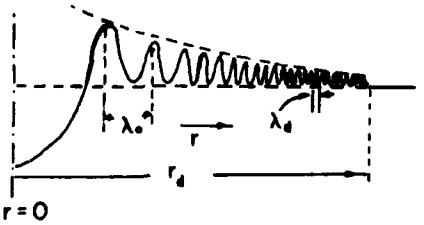

Fig. 7 - Schematic presentation of a crossection through the crater in Sn.

The measured values of the wave length near the crater λ_o, the value of λ_d and decay distance r_d (as defined in Figure 7) are as follows:

$$\lambda_o \simeq 20 \times 10^{-4} \text{ cm.}$$

$$\lambda_d \simeq 1.5 \times 10^{-4} \text{ cm.}$$

$$r_d \simeq 400 \times 10^{-4} \text{ cm.}$$

The sound wave velocity in Sn at room temperature is 2.5×10^5 cm/sec. Assuming that the elastic wave propagates at this velocity, when the shock wave is produced, we can obtain a time t for the propagation of this wave to a distance λ_o. This time t is calculated to be $\sim 8 \times 10^{-9}$ sec. This time compares favorably with the laser pulse rise time of the order of 10×10^{-9} sec. Similarly, the time t_d corresponding to the decay of the stress pulse amplitude is calculated to be $\sim 160 \times 10^{-9}$ sec.

It is realized that the material near the edge of the crater is heated to a temperature $\leq T_m$, where T_m is the melting point. Although, the temperature distribution $T(r,t)$ is not known, it can be assumed that an exponential decay type radial temperature distribution exists during the shock wave propagation through the material. Since the sound wave velocity and elastic moduli are inverse functions of the temperature, the wave propagates through a material where the modulus varies continuously. This could then account for the decay of λ. Two effects could account for the amplitude decay on the other hand. One is the dissipation of elastic energy in plastic work as the wave front moves out and the other is that because of the higher temperature near the edge of the crater the yield stress of the metal is low and thus a given amount of distortional elastic energy can produce a greater plastic yielding. It must be pointed out that non-crystallographic nature of the plastic yielding implies a non-conservative nature of dislocation motion during a very high strain rate associated with the shock pulse. Figure 8, shows an optical micrograph of laser damaged Sn at a laser energy density of $\sim 10^7$ watts/cm^2. At this relatively lower energy density more twinning and less ripple patter is observed.

Fig. 8 - Optical micrograph of Laser damage in Sn. Fluence $\sim 10^7$ watts/cm^2

In Sn very little if any wave pattern was observed even at the highest energy density available ($\sim 10^9$ w/cm^2). Profuse twinning, however, was observed adjacent to the damage site. The difficulty of plastic deformation due to the limited slip system might account for this difference. In polycrystalline Bi, the ripple pattern was almost identical to that for Sn.

Figure 9 shows a scanning electron micrograph for a laser damaged (~10^9 w/cm^2 Bi. This micrograph shows the fine spacing of the wave pattern at r ≈ 200 μ.

Fig. 9 - Scanning electron micrograph of wavy pattern in Bi. Fluence ~ 10^9 watts/cm^2.

Microstructural Effects Associated Crater Formation

At laser energy densities ~ 10^9 w/cm^2, secondary molten craters at grain boundrites and tripple points, at distances up to 150 μm from the edge of the laser spot was observed in bulk Cu, electro-chemically polished and etched before laser irradiation. Figure 10 shows such an observation. The nature of such localized temperature spikes is not clearly understood at this time.

Fig. 10 - Secondary molten craters along grain boundries in a polycrystalline Cu. Fluence ~ 10^9 watts/cm^2.

In a fully martensitic, medium carbon (1040) steel, reversion to austenite was achieved within a concentric circular area around the laser spot. Within this reverted structure, profuse grain boundry melting and void formation was observed as shown in Figure 11.

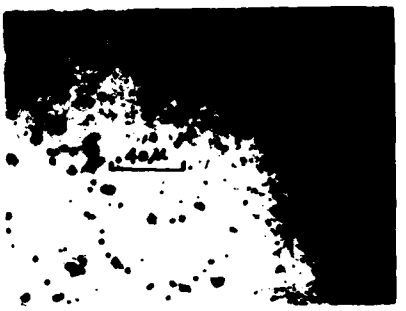

Fig. 11 - Void formation in reverted austenite in a 1040 steel. Fluence ~ 10^9 watts/cm^2.

Nature of Pulse Damage in Vapor Deposited Copper

Damage studies were carried out with ~ 2000 Å vapor deposited cupper foils which were backed up by an electro deposited Cu layer ~ 2mm thick. At identical laser energy fluences, the nature of the damage spot in the vapor deposited samples was quite different from that for the bulk Cu. The crater depth was almost uniform across the laser spot and no detectible slip, ripple pattern or liquid ejection were observed. It appears that the vapor deposited layer within the laser spot spalls and disintegrates rather than melts. Liquid metal ejection and bulk metal like behavior was, however, obtained after vacuum annealing which promoted grain growth in the vapor deposited layer.

Fig. 12 - Micro-void formation around the laser damaged spot in a vapor deposited Cu-foil.

One very interesting effect observed in the as received vapor deposited Cu foils is, that a halo of bluish-green color appeared within a few hours to a day in the laboratory atmosphere, around the laser damage craters produced at energy densities 10^9 w/cm^2. Areas away from the laser damage spot remained shiney. Microscopic observation revealed that a band of micro porosity deleniates this region as shown in Figure 12. It is concluded that there is a very high vacancy concentration and vacancy clusters in this region produced by the shock wave. High densities of ledge atoms and surface vacancies could provide activated sites for enhanced oxidation and corrosion in this region.

References

1. J. E. Michaels, Planetary and Space Science, Pergamon Press, NY, vol. 7 (1961).

2. R. M. White, J. Appl. Phys. 34, 2123 (1963).

3. N. M. Kroll, J. Appl. Phys. 36, 34 (1965).

4. S. S. Penner and O. P. Sharma, J. Appl. Phys., 37, 2304 (1966).

5. C. E. Bell and J. A. Landt, Appl. Phys. Lett 10, 46 (1967).

6. C. Mark Perceval, J. Appl. Phys., 38, 5313 (1967).

7. E. F. Carome, E. M. Carreira and C. J. Prochaska, Appl. Phys. Lett, 11, 64 (1967).

8. L. S. Gournay, J. Acoust. Soc. Am., 40, 1322 (1966).

9. J. C. Bushnell and D. J. McCloskey, J. App. Phys., 39, 12, 5541 (1968).

10. F. Haessner and W. Seitz, J. Mat. Science, 6, 16 (1971).

11. J. D. O'Keefe, C. H. Skeen and C. M. York, J. Appl. Phys., 44, 4622 (1973).

12. L. C. Yang, J. Appl. Phys., 45, 2601 (1974).

13. B. P. Fairand, A. H. Clauer, R. G. Jung and B. A. Wilcox, J. Appl. Phys., 25, 431 (1974).

14. Jay A. Fox, Appl. Phys. Lett., 24, 340 (1974).

15. B. Steverding and H. P. Dudel, J. Appl, Phys., 47, 1940 (1976).

16. J. D. Porteous, M. J. Soileau and C. W. Fountain, Appl. Phys. Lett., 29, 156 (1976).

17. J. D. Porteous, M. J. Soileau and C. W. Fountain, Laser Induced Damage in Optical Materials, NBS Special Publication, 462, p. 165 (1976).

18. J. D. Porteous, C. W. Fountain, J. L. Jernigan, W. N. Faith and H. E. Bennett, Laser Induced Damage in Optical Materials, NBS Special Publication, 509, p. 204 (1977).

19. O. T. Inal and L. E. Murr, J. Appl. Phys. 49, 2427 (1978).

20. R. A. Olstad and D. R. Olander, J. Appl. Phys., 46, 1499 (1975).

21. R. A. Olstad and D. R. Olander, J. Appl. Phys., 46, 1509 (1975).

22. H. Schwarz, Laser Interactions, Plenum Press, NY, (1971).

23. J. M. Baldwin, J. Appl. Phys., 44, 3362 (1973).

24. G. V. Plyatsko, N. I. Moisa and V. M. Khirovetskii, Sov. Mat. Science, (Eng. Trans.) 7, No. 3, 300 (1971).

25. V. G. Dneprovskii and B. A. Osadin, Sov. Phys. Tech. Phys., 19, No. 2, 275, (1974).

26. A. M. Bonch et. al., Sov. Phys. Tech. Phys., 19, No. 11, 1474, (1975).

27. S. I. Anisimov et al., Sov. Phys. Tech. Phys., 11, No. 7, 945 (1967).

28. I. G. Karasev et al., Sov. Phys. Tech. Phys., 15, No. 9, 1523 (1971).

29. W. A. Elliott, F. P. Gagliano and G. Krauss, Appl. Phys. Lett., 21, 23, (1972).

30. W. A. Elliott, F. P. Gagliano and G. Krauss, Met. Trans. 4, 2031 (1973).

31. B. H. Kear, E. M. Breinan and L. E. Greenwood, Materials Technology, April 1979, p. 121.

32. L. S. Weinman, C. Kim, T. R. Tuckey and E. A. Metzbower, Appl. Optics, 17, 906 (1978).

33. P. G. Moore & L. S. Weinman, SPIE, Vol. 198, Laser Applications in Materials Processing, p. 120 (1979).

34. J. Narayan, J. Metals, June 1980, p. 15.

35. A. E. H. Love, The Mathematical Theory of Elasticity, Dover press 1944.

36. D. W. Gregg and S. J. Thomas, J. Appl. Phys., 37, 2787 (1966).

37. R. J. Murphy & G. J. Ritter, Nature, April 9, 210, 191, (1966).

38. C. Vitali, M. Bestolotti, G. Foti and E. Rimini, Phys. Lett., 63A, 351 (1977).

39. J. C. Koo and R. E. Slusher, Appl. Phys. Lett., 28, No. 10, 614, (1976).

40. H. J. Leamy, G. A. Cazzenvi, F. T. Sheng and G. K. Celler, Appl. Phys. Lett., 32 (9), 556, (1978).

41. B. C. Emmony, R. F. Howson and L. J. Willis, Appl. Phys. Lett., 23, No. 11, 598, (1973).

42. L. E. Murr, O. T. Inal and A. A. Morales, Appl. Phys. Lett., 28, 432, (1976).

43. L. E. Murr, O. T. Inal and A. A. Morales, Acta. Met., 24, 261 (1976).

44. K. Mukherjee, T. H. Kim and W. T. Walter, to be published.